JOURNAL OF AIRCRAFT
Vol. 29, No. 4, July–Aug. 1992

Experimental-Theoretical Investigation of the Vibration Characteristics of Rotating Composite Box Beams

Ramesh Chandra* and Inderjit Chopra†
University of Maryland, College Park, Maryland 20742

This paper presents a theoretical-cum-experimental study of the free vibration characteristics of thin-walled composite box beams with bending-twist and extension-twist coupling under rotating conditions. The governing equations in generalized displacements were derived using a Newtonian approach. The composite structural model in the derivation used a solid-section approach and contained transverse shear-related couplings and appropriate cross-section warping. The free vibration characteristics of composite box beams were determined by the Galerkin method. In order to validate the theory, glass-epoxy, kevlar-epoxy and graphite-epoxy symmetric and antisymmetric box beams were fabricated using an autoclave molding technique, and tested in an in-vacuo rotor test facility for their vibration characteristics. Beam excitation in the rotating condition was effected by means of induced-strain actuation with the help of piezoceramic bending elements. Strain gages were used to measure the response of the first three modes over a range of rotational speeds up to 1000 rpm. It was determined that the experimental frequencies and mode shapes correlated satisfactorily with the theoretical results. It is shown also that bending-shear coupling influences the flexural vibration frequencies of antisymmetric box beams significantly. Extension-shear coupling, on the other hand, does not influence the flexural-torsion vibration frequencies of symmetric box beams significantly.

Nomenclature

A = cross-sectional area of blade
a, b = outer dimension of cross section of blade
I_{yy}, I_{zz} = blade cross section moment of inertia about y and z axes, respectively
K_{44} = torsional stiffness
K_{45} = bending-torsion (pitch-flap) coupling stiffness
K_{46} = bending-torsion (pitch-lag) coupling stiffness
K_{55} = bending stiffness corresponding to flap motion
K_{66} = bending stiffness corresponding to lag motion
K_A = effective polar radius of gyration of blade cross section $\sqrt{(I_{yy} + I_{zz})/A}$
K_m = $\sqrt{K_{m1}^2 + K_{m2}^2}$
K_{m1}, K_{m2} = principle mass radii of gyration of blade cross section
M_x = twisting moment about x axis
M_y = bending moment about y axis
M_z = bending moment about z axis
m = mass per unit length of blade
p_x, p_y, p_z = inertial forces
q_x, q_y, q_z = inertial moments
r = length of blade
t = time
u, v, w = elastic displacements in x, y, z directions, respectively
V_x = axial force in x direction
V_y, V_z = shear force in y and z directions, respectively
x, y, z = undeformed blade coordinates
β_y, β_z = rotations of cross section about y and z axes, respectively
$\varepsilon_{xx}, \varepsilon_{xy}, \varepsilon_{xz}$ = bending strain and cross section shear strains, respectively
$(\varepsilon_{xx})_m$ = maximum normal strain at the root of blade
ϕ = elastic twist of cross section of blade about shear center
Ω = rotational speed, rad/s
$\{\ \}^T$ = transpose
$(\ )_{,x}$ = $\partial/\partial x$

Introduction

THIN-walled composite beams with closed and open cross sections are widely used in the construction of helicopter rotor blades. Through the control of ply orientation and stacking sequence, structural couplings, such as bending-twist and extension-twist, are introduced. Hong and Chopra[1,2] showed that these elastic couplings had a significant influence on the aeroelastic performance of helicopter rotor blades. In the composite modeling used in those studies, the hollow cross section was treated as a general laminate very similar to a solid cross section. Hence the terminology used to describe symmetric and antisymmetric solid sections with respect to their mid axes was extended to hollow sections. Cross-section warping was assumed to depend upon the geometry of the cross section only, and transverse-shear and constrained warping effects were not included. In order to evaluate this composite structural beam model, Chandra et al.[3] conducted a systematic experimental and theoretical study on the static behavior of thin-walled graphite-epoxy box beams. In that investigation, symmetric and antisymmetric thin-walled composite box beams were fabricated using an autoclave molding technique and were tested under bending, torsional, and extensional loads. Theoretical results were obtained using the previously mentioned analytical beam model and a refined finite element method.[4] The correlation of the analytical, experimental, and finite element results showed that the composite beam model used by Hong and Chopra[1] was sufficiently accurate for antisymmetric (extension-twist coupled) beams

Received Nov. 5, 1990; revision received July 25, 1991; accepted for publication Aug. 29, 1991. Copyright © 1991 by the American Institute of Aeronautics and Astronautics, Inc. All rights reserved.

*Research Associate, Department of Aerospace Engineering. Member AIAA.
†Professor, Department of Aerospace Engineering. Fellow AIAA.

subjected to axial and torsional loads, whereas it was less satisfactory for symmetric (bending-twist coupled) beams. Smith and Chopra[5] then improved that beam model by including transverse shear effects and appropriate inplane elasticity. Also, the variation of shear stiffness in different walls of the section was included in the warping function. This model was extensively validated against static experimental data and refined finite element results.

Rehfield[6] and Rehfield et al.[7] presented a linear composite beam theory in which a contour analysis of the cross section was carried out and transvere-shear effects were included. Additional couplings due to transverse-shear were identified: bending-shear coupling for extension-twist coupled beams, and extension-shear coupling for bending-twist coupled beams. Restrained warping effects were included.

Nixon[8] investigated the efficacy of the coupled-beam analysis, Ref. 6, to predict the elastic twist requirements for full-scale extension-twist coupled tilt-rotor blades. He predicted the elastic twist of circular composite tubes representative of tilt-rotor blades under torsion and axial tension loads. The correlation with experimental data was satisfactory.

Hodges et al.[9] carried out an analytical investigation of the natural frequencies and mode shapes of composite beam structures. The beam equations were solved by two techniques: a transfer matrix method and a mixed finite element method. Vibration results were presented for solid beams and thin-walled circular cross-section beams. The investigation was confined to nonrotating beams.

The objective of this paper is to predict the influence of elastic couplings on the free vibration characteristics of thin-walled composite box beams and to correlate the results with experimental data. The theoretical results were calculated using Galerkin's method. The experimental data were obtained by testing graphite-epoxy, kevlar-epoxy, and glass-epoxy composite beams in an in-vacuo rotor test facility at different rotational speeds.

Analysis

The analysis is formulated to estimate the free vibration characteristics of rotating composite box beams with elastic coupling by means of small deflection theory. The analysis is intended for slender box beams, where direct transverse shear can be neglected, while retaining the structural couplings arising from transverse shear (bending-shear and extension-shear). The importance of these couplings has been demonstrated under static loading.[5,6] The bending-torsion vibrations of symmetric, and the bending vibration of antisymmetric beams, are studied. Extension-torsion vibrations are not included in the paper because the measurement of these high frequencies using piezoceramic device become difficult.

Equilibrium Equations

Figure 1 shows the forces and moments acting on a beam element. Following the works of Refs. 10 and 11, six equilibrium equations for beams under three moments and three forces, including inertial loadings, are obtained as

$$\frac{\partial M_x}{\partial x} + V_z\frac{\partial v}{\partial x} - V_y\frac{\partial w}{\partial x} + q_x = 0 \tag{1}$$

$$\frac{\partial M_y}{\partial x} + V_z - V_x\frac{\partial w}{\partial x} + q_y = 0 \tag{2}$$

$$\frac{\partial M_z}{\partial x} + V_y - V_x\frac{\partial v}{\partial x} + q_z = 0 \tag{3}$$

$$\frac{\partial V_x}{\partial x} + p_x = 0 \tag{4}$$

$$\frac{\partial V_y}{\partial x} + p_y = 0 \tag{5}$$

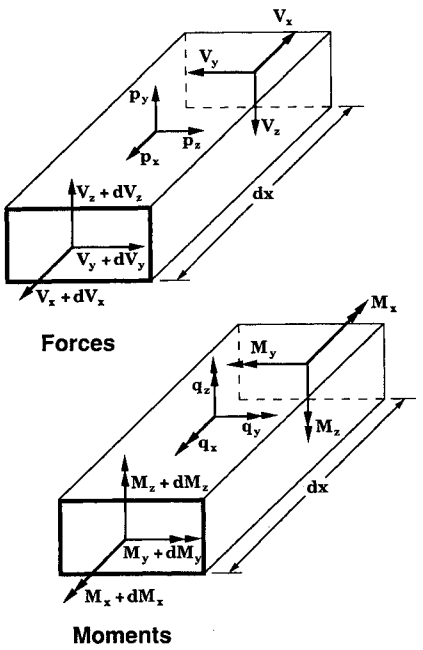

Fig. 1 Forces and moments acting on a beam element.

$$\frac{\partial V_z}{\partial x} + p_z = 0 \tag{6}$$

where

$$\begin{aligned} p_x &= m\Omega^2 x \\ p_y &= -m(v_{,tt} - \Omega^2 v) \\ p_z &= mw_{,tt} \\ q_x &= -mK_m^2\phi_{,tt} - \tfrac{1}{2}m\Omega^2(K_{m2}^2 - K_{m1}^2)\sin 2\phi \\ q_y &= 0 \\ q_z &= 0 \end{aligned} \tag{7}$$

The inertial loadings are specialized to untwisted uniform straight beams. For helicopter blades, several additional terms will be involved.

Eliminating V_y and V_z from Eqs. (1–6), the following flap, lag, torsion, and extension equations are obtained:

Flap

$$\frac{\partial^2 M_y}{\partial x^2} - \frac{\partial}{\partial x}\left(V_x\frac{\partial w}{\partial x}\right) - p_z = 0 \tag{8}$$

Lag

$$\frac{\partial^2 M_z}{\partial x^2} - \frac{\partial}{\partial x}\left(V_x\frac{\partial v}{\partial x}\right) - p_y = 0 \tag{9}$$

Torsion

$$\frac{\partial M_x}{\partial x} - \frac{\partial v}{\partial x}\frac{\partial M_y}{\partial x} + \frac{\partial w}{\partial x}\frac{\partial M_z}{\partial x} + q_x = 0 \tag{10}$$

Extension

$$\frac{\partial V_x}{\partial x} + p_x = 0 \tag{11}$$

It is important to note that the above four equations are valid in the regime of small deflection theory and in the ab-

sence of direct transverse shear deformation. The composite beam analysis is divided for simplicity into two parts, representing, respectively, symmetric and antisymmetric beams.

Symmetric Beam Analysis

These beams result in bending-torsion and extension-shear couplings. The composite structural model of Ref. 5 is used in the present study. This model includes the variation of shear modulus in different walls of the cross section in the warping function and transverse shear related couplings. However, restrained warping effects are not included in the model. It is shown in Ref. 3 that these effects are not important for the composite beams of the present investigation. The force-displacement relations are

$$\begin{Bmatrix} M_x \\ M_y \\ M_z \end{Bmatrix} = \begin{bmatrix} K_{44} & K_{45} & K_{46} \\ K_{45} & K_{55} & 0 \\ K_{46} & 0 & K_{66} \end{bmatrix} \begin{Bmatrix} \phi_{,x} \\ w_{,xx} - \varepsilon_{xz,x} \\ v_{,xx} - \varepsilon_{xy,x} \end{Bmatrix} \tag{12a}$$

$$\begin{Bmatrix} V_x \\ V_y \\ V_z \end{Bmatrix} = \begin{bmatrix} K_{11} & K_{12} & K_{13} \\ K_{12} & K_{22} & 0 \\ K_{13} & 0 & K_{33} \end{bmatrix} \begin{Bmatrix} u_{,x} \\ \varepsilon_{xy} \\ \varepsilon_{xz} \end{Bmatrix} \tag{12b}$$

where

$$\varepsilon_{xz} = w_{,x} - \beta_z$$

$$\varepsilon_{xy} = v_{,x} - \beta_y$$

The coefficients K_{ij} are defined in Ref. 5.

In the dynamic analysis, the terms $\varepsilon_{xy,x}$ and $\varepsilon_{xz,x}$ are nonzero because the nonuniform inertial loading, and therefore the bending, torsion, and shear are coupled. Also, for beams under rotation the torsional stiffness term K_{44}[10] becomes $(K_{44} + V_x K_A^2)$. Substituting relations Eq. (12a) into relations (8–10), the following linearized governing equations are obtained:

Flap

$$K_{55}\frac{\partial^4 w}{\partial x^4} + K_{45}\frac{\partial^3 \phi}{\partial x^3} + m\frac{\partial^2 w}{\partial t^2} - \frac{1}{2}m\Omega^2\frac{\partial}{\partial x}\left[\frac{\partial w}{\partial x}(r^2 - x^2)\right] = 0 \tag{13}$$

Lag

$$K_{66}\frac{\partial^4 v}{\partial x^4} + K_{46}\frac{\partial^3 \phi}{\partial x^3} + m\frac{\partial^2 v}{\partial t^2} - m\Omega^2 v - \frac{1}{2}m\Omega^2\frac{\partial}{\partial x}\left[\frac{\partial v}{\partial x}(r^2 - x^2)\right] + m\Omega^2 K_{66}L_{22}\frac{\partial^2 v}{\partial x^2} = 0 \tag{14}$$

Torsion

$$K_{44}\frac{\partial^2 \phi}{\partial x^2} + K_{45}\frac{\partial^3 w}{\partial x^3} + K_{46}\frac{\partial^3 v}{\partial x^3} - mK_m^2\frac{\partial^2 \phi}{\partial t^2} - m\Omega^2(K_{m2}^2 - K_{m1}^2)\phi + \frac{1}{2}m\Omega^2 K_A^2\frac{\partial}{\partial x}\left[\frac{\partial \phi}{\partial x}(r^2 - x^2)\right] + m\Omega^2 K_{46}L_{22}\frac{\partial v}{\partial x} = 0 \tag{15}$$

L_{22} is obtained by inverting Eq. (12b)

$$[L] = [K]^{-1}$$

Note that the derivation of these equations does not include the influence of extension-shear coupling on the initial state (before vibration); it is believed to be a higher order effect. Also, the transverse shear strains ε_{xz} and ε_{xy} are eliminated in the derivation by inverting Eq. (12b). Thus, these equations include extension-transverse shear coupling.

Solution

For a cantilevered beam including direct transverse shear deformation, the root conditions are

$$w = 0, \quad v = 0, \quad \phi = 0, \quad \beta_y = 0, \quad \beta_z = 0 \tag{16}$$

Because the direct transverse shear effect is neglected in the present analysis, the root conditions are reduced to

$$w = 0, \quad v = 0, \quad \phi = 0, \quad w_{,x} = 0, \quad v_{,x} = 0 \tag{17}$$

This implies that the cross section shear strains are retained in the analysis.

The coupled differential equations are solved by using Galerkin's method. The displacements w, v, and ϕ are assumed as

$$w = \sum_{i=1}^{n} a_i\psi_i \tag{18}$$

$$v = \sum_{i=1}^{n} b_i\psi_i \tag{19}$$

$$\phi = \sum_{i=1}^{n} c_i \sin\left(\frac{2i-1}{2}\frac{\pi x}{r}\right) \tag{20}$$

where ψ_i are beam functions. For a cantilevered beam

$$\psi_i = \cosh\frac{\lambda_i x}{r} - \cos\frac{\lambda_i x}{r} - \alpha_i\left(\sinh\frac{\lambda_i x}{r} - \sin\frac{\lambda_i x}{r}\right)$$

These functions satisfy the kinematic and force boundary conditions of the cantilever beam. Applying Galerkin's method to Eqs. (13–15)

$$\begin{aligned} m\{a\}_{,tt} + [K_f]\{a\} + [K_{ft}]\{c\} &= 0 \\ m\{b\}_{,tt} + [K_l]\{b\} + [K_{lt}]\{c\} &= 0 \\ mK_m^2\{c\}_{,tt} + [K_t]\{c\} + [K_{tf}]\{a\} + [K_{tl}]\{b\} &= 0 \end{aligned} \tag{21}$$

where

$$\{a\} = \{a_1, a_2, a_3, \ldots a_n\}^T$$

$$\{b\} = \{b_1, b_2, b_3, \ldots b_n\}^T$$

$$\{c\} = \{c_1, c_2, c_3, \ldots c_n\}^T$$

$$[K_f] = \frac{K_{55}}{r^4}[\lambda] - \frac{m\Omega^2}{2r}[I_2]^T + \frac{m\Omega^2}{r}[I_3]^T$$

$$[K_{ft}] = -\frac{\pi^3}{8r^4}K_{45}[I_1]^T$$

$$[K_l] = \frac{K_{66}}{r^4}[\lambda] - m\Omega^2[I] - \frac{m\Omega^2}{2r}[I_2]^T + \frac{m\Omega^2}{r}[I_3]^T + \frac{m\Omega^2}{r}K_{66}L_{22}[I_7]^T$$

$$[K_{lt}] = -\frac{\pi^3}{8r^4} K_{46}[I_1]^T$$

$$[K_l] = \frac{\pi^2}{4r^2} K_{44}[J] - m\Omega^2(K_{m2}^2 - K_{m1}^2)[I] + \frac{\pi^2}{4} m\Omega^2 \frac{K_A^2}{r^3}[I_5]^T - \frac{\pi^2}{4} m\Omega^2 \frac{K_A^2}{r^2}[I_6]^T$$

$$[K_{tf}] = -\frac{2}{r} K_{45}[I_4]^T$$

$$[K_{tl}] = -\frac{2}{r} K_{46}[I_4]^T - \frac{2m\Omega^2}{r} K_{46}K_{22}[I_8]^T \tag{22}$$

Matrices $[I_1]$–$[I_8]$, $[\lambda]$, $[J]$ and $[I]$ are defined in the Appendix.

The coupled linear differential Eqs. (21) are solved as an algebraic eigenvalue problem. Using the kinematic relations of Ref. 5, the strain mode shapes (bending and torsional shear) are computed

$$\frac{\varepsilon_{xx}}{(\varepsilon_{xx})_m} = \frac{b}{(\varepsilon_{xx})_m} \sum_{i=1}^{n} a_i \psi_{i,xx}(x)$$

$$\frac{\varepsilon_{xy}}{(\varepsilon_{xx})_m} = \frac{b^2}{(a+b)(\varepsilon_{xx})_m} \sum_{i=1}^{n} c_i \left(\frac{2i-1}{2}\frac{\pi}{r}\right) \cos\frac{2i-1}{2}\frac{\pi x}{r} \tag{23}$$

where

$$(\varepsilon_{xx})_m = \frac{b}{r^2} \sum_{i=1}^{n} a_i \lambda_i^2 \tag{24}$$

Antisymmetric Beam Analysis

These beam configurations result in extension-torsion and bending-shear couplings. The force-displacement relations are taken from Ref. 5

Extension-torsion

$$\begin{Bmatrix} V_x \\ M_x \end{Bmatrix} = \begin{bmatrix} K_{11} & K_{14} \\ K_{14} & K_{44} \end{bmatrix} \begin{Bmatrix} u_{,x} \\ \phi_{,x} \end{Bmatrix} \tag{25}$$

Flap bending moment-lag transverse shear

$$\begin{Bmatrix} V_y \\ M_y \end{Bmatrix} = \begin{bmatrix} K_{22} & K_{25} \\ K_{25} & K_{55} \end{bmatrix} \begin{Bmatrix} \varepsilon_{xy} \\ w_{,xx} - \varepsilon_{xz,x} \end{Bmatrix} \tag{26}$$

Lap bending moment-flap transverse shear

$$\begin{Bmatrix} V_z \\ M_z \end{Bmatrix} = \begin{bmatrix} K_{33} & K_{36} \\ K_{36} & K_{66} \end{bmatrix} \begin{Bmatrix} \varepsilon_{xz} \\ v_{,xx} - \varepsilon_{xy,z} \end{Bmatrix} \tag{27}$$

Because this study is confined to bending vibrations, and because bending-twist coupling is zero for these beams, relation (25) is not used. As seen from relations (26) and (27), bending moment and transverse shear are coupled. To further simplify the analysis, the transverse shear strains are not included as degrees of freedom. By eliminating ε_{xy} and ε_{xz} from the force-displacement relations, the bending moments are expressed in terms of transverse displacements.

Inverting Eqs. (26) and (27) results in

$$\begin{aligned} \varepsilon_{xy} &= L_{22}V_y + L_{25}M_y \\ \varepsilon_{xz} &= L_{33}V_z + L_{36}M_z \end{aligned} \tag{28}$$

where

$$L_{22} = -\frac{K_{55}}{K_{25}^2 - K_{22}K_{55}}; \qquad L_{25} = \frac{K_{25}}{K_{25}^2 - K_{22}K_{55}}$$

$$L_{33} = -\frac{K_{66}}{K_{36}^2 - K_{33}K_{66}}; \qquad L_{36} = \frac{K_{36}}{K_{36}^2 - K_{33}K_{66}}$$

Using relations (26–28), M_y and M_z are obtained as

$$\begin{aligned} M_y &= f_1V_y + f_2w_{,xx} + f_3V_{z,x} + f_4M_{z,x} \\ M_z &= g_1V_z + g_2v_{,xx} + g_3V_{y,x} + g_4M_{y,x} \end{aligned} \tag{29}$$

where

$$f_1 = \frac{K_{25}L_{22}}{1 - K_{25}L_{25}}; \qquad f_2 = \frac{K_{55}}{1 - K_{25}L_{25}}$$

$$f_3 = -\frac{K_{55}L_{33}}{1 - K_{25}L_{25}}; \qquad f_4 = \frac{K_{55}}{1 - K_{25}L_{25}} \tag{30}$$

$$g_1 = \frac{K_{36}L_{33}}{1 - K_{36}L_{36}}; \qquad g_2 = \frac{K_{66}}{1 - K_{36}L_{36}}$$

$$g_3 = -\frac{K_{66}L_{22}}{1 - K_{36}L_{36}}; \qquad g_4 = -\frac{K_{66}L_{25}}{1 - K_{36}L_{36}}$$

Using relations (27) in equilibrium Eqs. (8) and (9), the governing equations in flap and lag directions are obtained.

Flap

$$m\frac{\partial^2 w}{\partial t^2} + f_2\frac{\partial^4 w}{\partial x^4} - \frac{1}{2}m\Omega^2\frac{\partial}{\partial x}\left[\frac{\partial w}{\partial x}(r^2 - x^2)\right] - f_4\frac{1}{2}m\Omega^2\frac{\partial^2}{\partial x^2}\left[\frac{\partial v}{\partial x}(r^2 - x^2)\right] + (f_1 - f_4)\,m\Omega^2\frac{\partial v}{\partial x} = 0 \tag{31}$$

Lag

$$m\frac{\partial^2 v}{\partial t^2} + g_2\frac{\partial^4 v}{\partial x^4} - \frac{1}{2}m\Omega^2\frac{\partial}{\partial x}\left[\frac{\partial v}{\partial x}(r^2 - x^2)\right] - g_3m\Omega^2\frac{\partial^2 v}{\partial x^2} - m\Omega^2 v - g_4\frac{1}{2}m\Omega^2\frac{\partial^2}{\partial x^2}\left[\frac{\partial w}{\partial x}(r^2 - x^2)\right] = 0 \tag{32}$$

It is important to note that the derivation of these equations does not include the influence of extension-twist coupling on the previbration state of the beam. These coupled equations are solved using Galerkin's method. Beam functions with three terms given by relations (18) and (19) were used.

In Vacuo Rotor Test Facility

The experimental data were obtained in the in vacuo rotor test facility, one in which rotor models can be tested at different rotational speeds in the absence of aerodynamic forces. The facility is used to advance the understanding of the structural couplings of composite rotors, of inertial coupling of rotor/body systems, and of the dynamic response of advanced rotor systems under a prescribed loading. In the present paper, the facility is used to validate the theoretical vibration characteristics of thin-walled composite beams with structural couplings at different rotational speeds.

The facility consists of a 10-ft diam. by 4-ft-high vacuum chamber, a rotary vane vacuum pump of 120 ft³/min capacity, a variable speed dc motor with controller, and a 100 channel slip ring. Figure 2 shows the schematic diagram of the facility. A vacuum level of the order of 4 mbars, can be achieved in about 45 min. The rotational speed is sensed by a photo cell and can be controlled within ±1% accuracy. A hub was designed to provide clamped conditions in the flap and lag directions for a four-bladed rotor. In the present study, a two-bladed rotor was used.

Piezoelectric Actuator Excitation System

The excitation of rotating beams in the vacuum chamber is provided by means of piezoelectric devices. This type of strain-induced actuation was also employed by other researchers[12,13] to determine the vibration characteristics of beams. The performance of a strain-induced piezoactuator is defined in terms of a parameter called 'piezoelectric mechanical coupling effectiveness.' This nondimensional parameter represents the maximum amount of induced strain that a piezoactuator can transmit to the substructure under ideally-bonded static conditions when a maximum allowable field is applied across the piezodevice. The parameter depends upon the piezoelectric constant (material property), the maximum allowable field, and the stiffness ratio of actuator to substructure. Piezoelectric ceramics (G-1195 manufactured by Piezo Electric Products) have a high coupling effectiveness[13] and were therefore selected for this work.

Actuator location is an important issue for exciting the beams. The actuators must be placed at locations where the strains are high when the beam is vibrating in one of its natural modes and should not be placed at zero crossing points of the strain modes (equivalent to nodes in displacement mode). The strain mode represents the variation of strain along the length of the beam. In the present study, the piezoceramic actuators are placed near the clamped end of the rotor blade because the modes of interest were the first and second cantilever modes.

Three considerations were involved in the surface mounting of the piezoceramic actuators onto the composite beams. Electrical contact has to be made with both faces of the piezo element after bonding, the piezoelements needed to be electrically insulated from the structure, and bonding had to be of uniform thickness. To achieve these requirements, a one-sided copper clad sheet (conducting on one side and insulating on the other) is placed between the piezoelement and the structure (Fig. 3). M bond adhesive from Measurement Group is used to bond the actuator and the sheet. This adhesive provides close to an ideal bonding because of its special characteristics (i.e., high shear stiffness and thin bond line).

Several piezoceramic elements are needed to excite composite beams in different modes, such as flap, lag, and torsion,

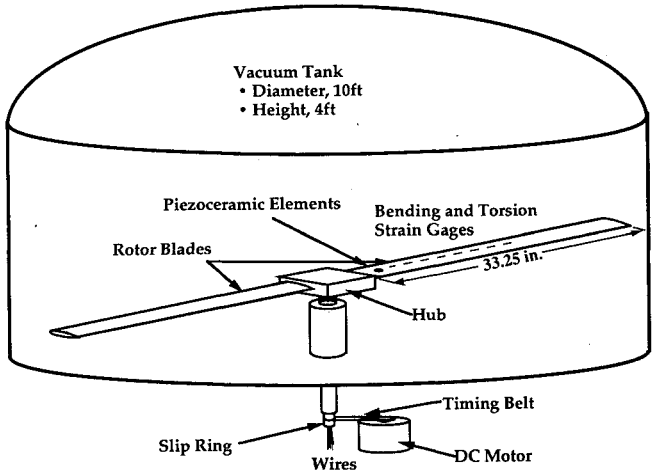

Fig. 2 Schematic of in-vacuo rotor test facility.

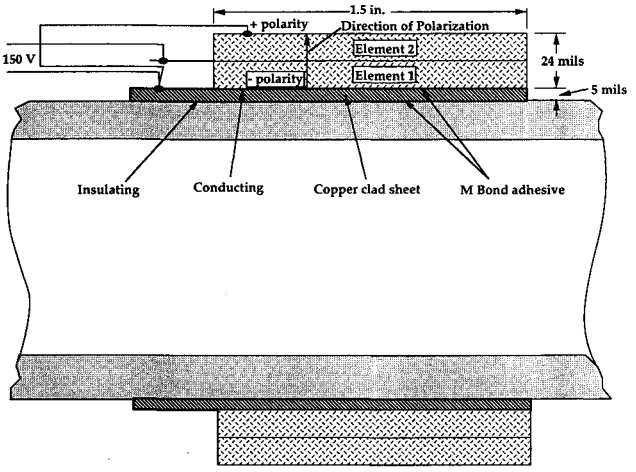

Fig. 3 Surface mounting of piezoceramic bender elements on box beams.

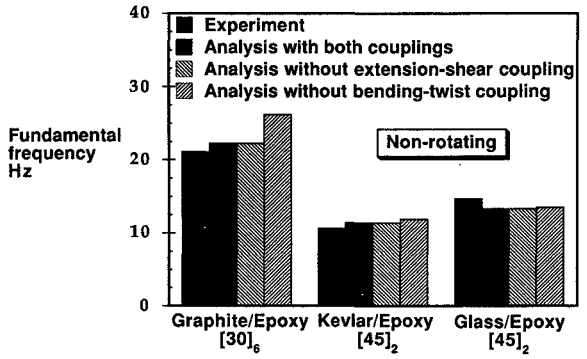

Fig. 4 Analytical and experimental fundamental frequencies of non-rotating symmetric box beams.

and one pair of elements each for flap and lag modes is used. Two elements of a pair are surface-mounted on opposite sides of the box beam (top and bottom for flap and left and right for lag).

Instrumentation

Special instrumentation to control the phase and amplitude of the excitation forces was developed in-house for multipoint excitation. The response of the rotor blades was monitored by means of strain gages and accelerometers. A 100-channel slip ring was used to transmit signals between the piezoelectric actuators and the other transducers mounted on the beams in the rotating frame, and the vibration control and analysis equipment placed outside the vacuum chamber. An HP1000 microcomputer was used to control the excitation forces, and a multi-channel 6080/6081 spectrum analyzer was used to extract modal parameters.

Dynamic Testing

In order to establish the validity of vibration testing in the vacuum chamber, a two-bladed aluminum rotor was tested first. The blade consisted of a solid rectangular section beam (2-in. wide and 0.063-in. thick) of 36-in. length, and was excited by a single piezoelectric bending element. Its response was measured by a single bending strain gage. A sine sweep excitation was used to search for natural frequencies corresponding to the first three modes. The correlation between experimental and theoretical frequencies for all three modes was good.

Graphite-epoxy, kevlar-epoxy, and glass-epoxy box beams of different lay-ups were built using an autoclave molding technique; the fabrication details of the box beams are given in Ref. 3. Table 1 shows the details of these beam specimens which were tested in the vacuum chamber facility for their

Table 1 Details of thin-walled composite box beams

Material	Mechanical properties E_L, 10^6 psi	E_T, 10^6 psi	G_{LT}, 10^6 psi	μ_{LT}	Configuration	Flanges Top	Flanges Bottom	Webs Left	Webs Right
					Symmetric 1	$[30]_6$	$[30]_6$	$[\pm 30]_3$	$[\pm 30]_3$
					Symmetric 2	$[45]_6$	$[45]_6$	$[\pm 45]_3$	$[\pm 45]_3$
Graphite-epoxy	20.59	1.42	0.89	0.42	Antisymmetric 1	$[15]_6$	$[-15]_6$	$[15]_6$	$[-15]_6$
					Antisymmetric 2	$[0/30]_3$	$[0/-30]_3$	$[0/30]_3$	$[0/-30]_3$
					Antisymmetric 3	$[0/45]_3$	$[0/-45]_3$	$[0/-45]_3$	$[0/45]_3$
Kevlar-epoxy	11	0.8	0.34	0.34	Symmetric 3	$[45]_2$	$[45]_2$	± 45	± 45
Glass-epoxy	7	2.1	0.8	0.26	Symmetric 4	$[45]_2$	$[45]_2$	± 45	± 45

Geometry of beam: length = 33.25 in.; inner dimensions of the cross section = 0.893 × 0.477 in.
Graphite-epoxy beams: ply thickness = 0.005 in., wall thickness = 0.030 in., no. of layers = 6, mass density = 0.1352 × 10^{-3} lb s^2/in.^{4}
Kevlar-epoxy beams: ply thickness = 0.010 in., wall thickness = 0.020 in., no. of layers = 2, mass density = 0.1042 × 10^{-3} lb s^2/in.^{4}
Glass-epoxy beams: ply thickness = 0.016 in., wall thickness = 0.032 in., no. of layers = 2, mass density = 0.1676 × 10^{-3} lb s^2/in.^{4}

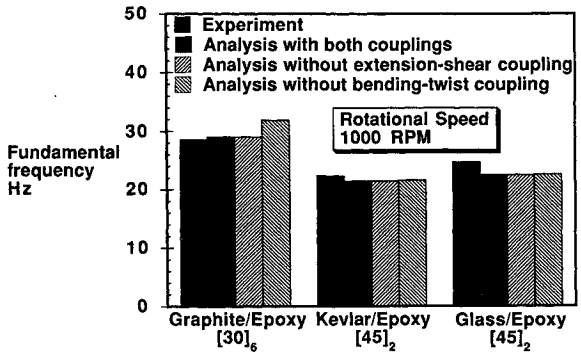

Fig. 5 Analytical and experimental fundamental frequencies of symmetric box beams at rotational speed of 1000 rpm.

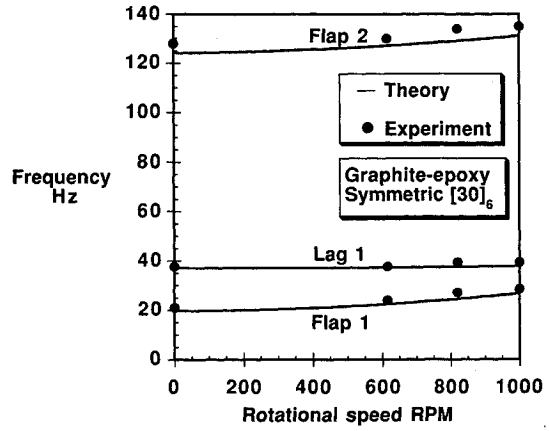

Fig. 6 Natural frequencies of $[30]_6$ graphite-epoxy symmetric box beams at various rotational speeds.

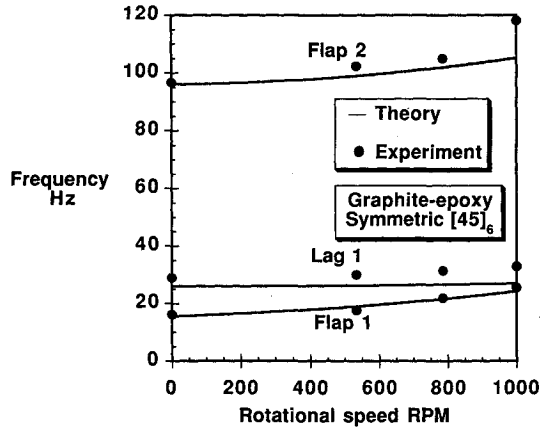

Fig. 7 Natural frequencies of $[45]_6$ graphite-epoxy symmetric box beams at various rotational speeds.

vibration characteristics. Excitation was provided by two pairs of piezoceramic elements, one pair each for the flap and lag modes. The pairs were driven by sinusoidal signals with a maximum amplitude of ±150 V, and the phase difference between the electric signals to the elements on opposite surfaces of a pair was 180 deg. Four strain gages were bonded on two piezoceramic elements to provide the induced strain signal which was used as an input function for the determination of the frequency response function for the extraction of modal parameters. In order to reduce the noise to signal ratio, full four-armed strain gage bridges for flap, lag, and torsion responses were used. The flap and torsion bridges were bonded at four different spanwise locations to measure mode shapes. Thus, the amplitudes and frequencies from eight (four bending and four torsion) strain gages, bonded at different locations along the beam, were obtained for a range of rotational speeds varying from 0 to 1000 rpm. The bending and torsion strain mode shapes were derived by normalizing the strain amplitude with respect to the extrapolated value of bending strain amplitude at the root. A quadratic polynomial curve fitting for the strain amplitude data was used to obtain the value of strain amplitude at the root.

Results and Discussion

Table 1 shows the details of the composite box beams of the present investigation with respect to geometry, layup, material properties, and wall thickness. These beams of uniform cross section are mounted as cantilevers for dynamic testing. For Galerkin's solution, three terms of beam functions, respectively each for flap, lag, and torsion were used. The numerical integration was carried out using the Gauss-Legendre quadrature formula.

Symmetric Beams

Figure 4 presents the influence of bending-twist and extension-shear coupling on calculated values of nonrotating fundamental frequencies for graphite-epoxy $[30]_6$, kevlar-epoxy $[45]_2$, and glass-epoxy $[45]_2$ box beams. Bending-twist coupling reduces the frequency, the reduction depending upon the material and layup of the beam. Also, this coupling causes bending-torsion coupled modes. The effect of extension-shear coupling on the first frequency of these beams is insignificant. Good correlation between experiment and theory is seen. Figure 5 shows similar results for these beams rotating at 1000 rpm. The influence of bending-twist coupling on the fundamental frequency of rotating beams becomes smaller because the rotating beam derives a good part of its stiffness from centrifugal force. Good correlation between theory and experiment is seen in Fig. 5 for rotating beams also.

Figure 6 shows the influence of rotation on the theoretical and experimental values of the first three natural frequencies (the first two flap and the first lag) for $[30]_6$ symmetric graphite-epoxy beams. The test beam has bending-torsion coupling, and hence the flap 1, flap 2, and lag 1 modes indicated in the figure correspond to coupled modes with predominant flag

and lag motions. The correlation between theoretical and experimental results is within 7%. The maximum increase in frequency resulting from rotation occurs for the first flap mode and is about 36% at 1000 rpm. Figure 7 shows similar results for $[45]_6$ symmetric graphite-epoxy beams. The correlation between theoretical and experimental results for the test beam is within 10%. This deviation is plausibly due to inaccuracies in the prediction of stiffness coefficients for 45-deg beams in the structural model.[5] The increase in first frequency due to rotation for this beam is 68% at 1000 rpm.

Figure 8 shows the influence of rotational speed on the first three frequencies of symmetric $[45]_2$ kevlar-epoxy box beams. An increase of about 100% in fundamental frequency at 1000 rpm is shown. The correlation of theoretical and experimental results is within 10%. Figure 9 illustrates the first mode shape for this beam, wherein the amplitude is normalized with respect to the maximum bending strain at the root of the blade. Because of structural coupling, the fundamental mode is a coupled bending-torsion mode. The maximum torsional strain is about 25% of the maximum bending strain. The correlation between theory and experiment for the mode shape is good. Because of low values of strain towards the tip, measured values beyond 50% of the span are not presented. It is to be noted that the rotational speed up to 1000 rpm does not influence the mode shape of this beam.

Figure 10 shows the theoretical and experimental values of first three frequencies for a symmetric $[45]_2$ glass-epoxy beam at various rotational speeds. For this beam, there is an increase of 70% in first bending frequency at 1000 rpm. The correlation of theoretical and experimental results is within 10%. The coupled bending-torsion strain modes for this beam with and without rotation were also obtained. Good correlation between theory and experiment was achieved for this beam configuration, also. Thus for all symmetric layup beams which exhibit bending-torsion coupling, the correlation between theoretical and experimental values of the first two frequencies is within 10%. Bending-torsion coupling affects the frequencies via a reduction in direct stiffness.

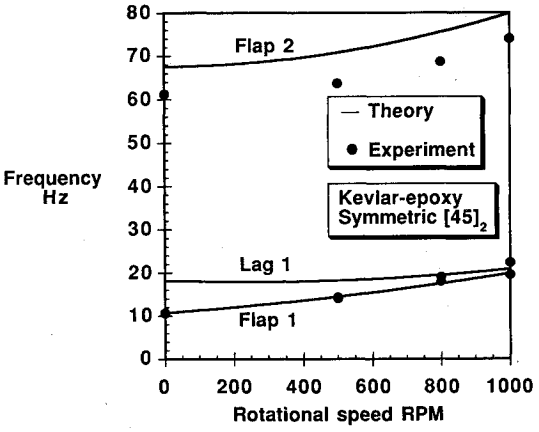

Fig. 8 Natural frequencies of $[45]_2$ kevlar-epoxy symmetric box beams at various rotational speeds.

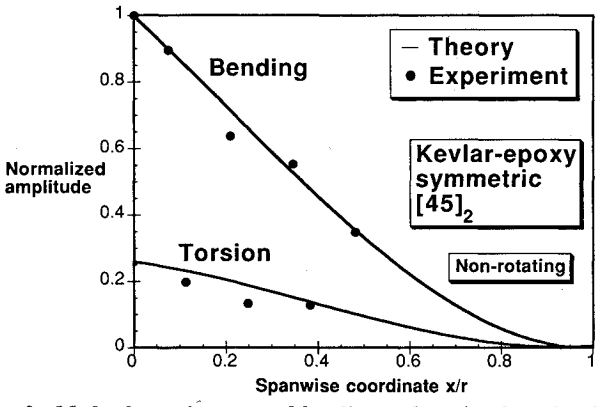

Fig. 9 Mode shapes in terms of bending and torsional strain of a nonrotating $[45]_2$ kevlar-epoxy symmetric box beam.

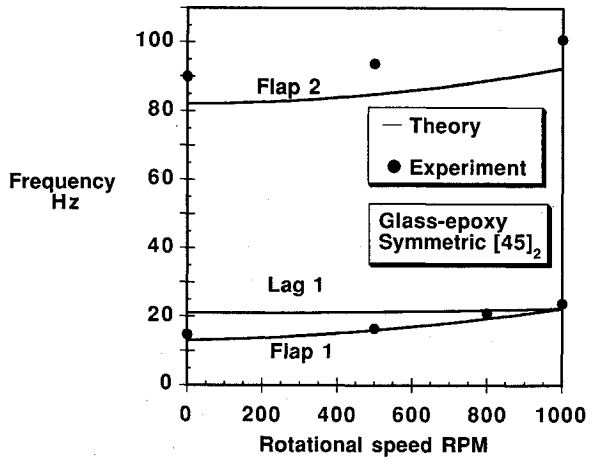

Fig. 10 Natural frequencies of $[45]_2$ glass-epoxy symmetric box beams at various rotational speeds.

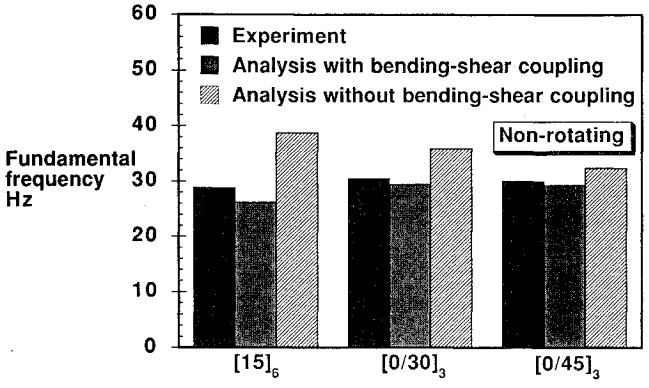

Fig. 11 Analytical and experimental values of fundamental frequencies of nonrotating antisymmetric box beams.

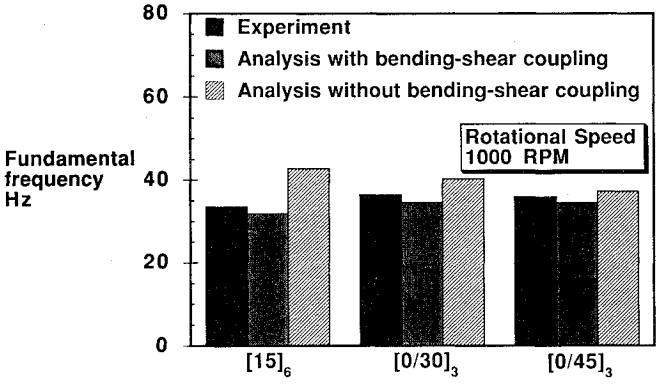

Fig. 12 Analytical and experimental fundamental frequencies of antisymmetric box beams at rotational speed of 1000 rpm.

Antisymmetric Beams

Figure 11 shows the influence of bending-shear coupling on the fundamental frequencies of nonrotating graphite-epoxy antisymmetric beams. The influence of coupling on the frequencies is seen to be very significant for $[15]_6$ beams, because the value of bending-shear coupling stiffness is more for this beam in comparison with $[0/30]_3$ and $[0/45]_3$ beams, respectively. The omission of bending-shear coupling for the computation of natural frequencies overestimates the fundamental frequencies by around 40% for $[15]_6$ beams. Good correlation between experiment and analysis with bending-shear coupling can be seen for these beams. Figure 12 shows the influence of bending-shear coupling on the fundamental frequencies of rotating (1000 rpm) antisymmetric graphite-epoxy box

beams, where it can be seen that the reduction in frequencies resulting from this coupling is less severe on comparison with nonrotating beams. Again, there is good correlation between experiment and analysis. The influence of rotational speed on the first three frequencies (first flap, first lag, and second flap) of these antisymmetric box beams was not significant because of their high stiffnesses. The correlation between theory and experiment at various rotational speeds is again within 10%. The increase in the first flap frequency due to the rotation for these beams is of the order of 17% at 1000 rpm.

Measurement of displacement mode shapes poses some problems, although mode shapes can be obtained by using ultralight accelerometers. For this purpose, piezoresistive accelerometers of 0.5 g weight from Entran (EGAX) were used. Four accelerometers were adhesive bonded onto the rotor blade with the help of M Bond adhesive from Measurement Group. FFT analyses of the accelerometer signals provided the amplitude versus frequency plots. The amplitudes thus obtained were normalized with respect to the tip amplitude, and mode shapes were obtained. Because of the problems associated with reusing these expensive transducers with adhesive bonding, their application for further composite beam specimens was abandoned. For this beam, rotations up to 1000 rpm did not influence the mode shape.

Conclusions

The coupled flap-lag-torsion equations for composite thin-walled beams were derived by using a Newtonian approach. The force-displacement relations used in the derivation included an appropriate representation of cross-sectional warping and transverse shear-related couplings. Theoretical values of free vibration characteristics of coupled thin-walled composite beams under rotation were determined by applying Galerkin's method. A 10-ft-diam vacuum chamber test facility was used successfully to determine the experimental vibration characteristics of thin-walled symmetric and antisymmetric composite beams at various rotational speeds (maximum 1000 rpm). Good quality beam specimens were built out of graphite-epoxy, kevlar-epoxy, and glass-epoxy laminae using an autoclave molding technique. The beams were excited by piezoceramic elements attached near the root end, and sufficient forcing level was achieved to identify the first two flap bending modes and the fundamental lag mode. Strain as well as displacement mode shapes were determined. Acceptable correlations between the measured frequencies and modes with theoretical results were achieved.

Based on this study, the following conclusions are drawn:

1) Bending-twist coupling for symmetric beams reduce their frequencies and create bending-torsion coupled modes. The magnitude of the coupling of modes depends upon the layup and material of the beams. For kevlar-epoxy $[45]_2$ beams, the maximum torsional strain is around 25% of the maximum bending strain in the first mode. Extension-shear coupling does not influence the first three natural frequencies of symmetric beams. Rotation reduces the influence of bending-twist coupling on the natural frequencies of symmetric beams.

2) Bending-shear coupling in antisymmetric beams reduce their frequencies and create flap-lag coupled modes. The influence of such coupling on free vibration characteristics is very significant and must be included in the analysis. For graphite-epoxy $[15]_6$ antisymmetric beams, this coupling reduces the fundamental frequency by about 40%. Rotation reduces the influence of bending-shear coupling on the natural frequencies of antisymmetric beams.

Appendix: Matrices $[\lambda]$, $[J]$, $[I]$ and $[I_1]$–$[I_8]$

$$[\lambda] \equiv \begin{bmatrix} \lambda_1^4 & 0 & 0 \\ 0 & \lambda_2^4 & 0 \\ 0 & 0 & \lambda_3^4 \end{bmatrix}; \quad [J] \equiv \begin{bmatrix} 1 & 0 & 0 \\ 0 & 9 & 0 \\ 0 & 0 & 25 \end{bmatrix}; \quad [I] \equiv \begin{bmatrix} 1 & 0 & 0 \\ 0 & 1 & 0 \\ 0 & 0 & 1 \end{bmatrix}$$

$$I_{1ij} = \int_0^r (2i - 1)^3 \cos\left(\frac{2i - 1}{2}\frac{\pi x}{r}\right) \psi_j \, dx$$

$$I_{2ij} = \int_0^r (r^2 - x^2)\, \psi_{i,xx}\psi_j \, dx$$

$$I_{3ij} = \int_0^r x\psi_{i,x}\psi_j \, dx$$

$$I_{4ij} = \int_0^r \psi_{i,xxx} \sin\left(\frac{2j - 1}{2}\frac{\pi x}{r}\right) dx$$

$$I_{5ij} = \int_0^r \sin\left(\frac{2i - 1}{2}\frac{\pi x}{r}\right) \sin\left(\frac{2j - 1}{2}\frac{\pi x}{r}\right) \cdot (2i - 1)^2 (r^2 - x^2) \, dx$$

$$I_{6ij} = \int_0^r \cos\left(\frac{2i-1}{2}\frac{\pi x}{r}\right) \sin\left(\frac{2j - 1}{2}\frac{\pi x}{r}\right) \cdot (2i - 1)x \, dx$$

$$I_{7ij} = \int_0^r \psi_{i,xx}\psi_j \, dx$$

$$I_{8ij} = \int_0^r \psi_{i,x} \sin\left(\frac{2j - 1}{2}\frac{\pi x}{r}\right) dx$$

References

[1]Hong, C. H., and Chopra, I., "Aeroelastic Stability of a Composite Blade," *Journal of the American Helicopter Society,* Vol. 30, No. 2, 1985, pp. 57–67.

[2]Hong, C. H., and Chopra, I., "Aeroelastic Stability Analysis of a Composite Bearingless Rotor Blade," *Journal of the American Helicopter Society,* Vol. 31, No. 4, 1986, pp. 29–35.

[3]Chandra, R., Stemple, A., and Chopra I., "Thin-Walled Composite Beams under Bending, Torsional and Extensional Loads," *Journal of Aircraft,* Vol. 27, No. 7, 1990, pp. 619–627.

[4]Stemple, A. D., and Lee, S. W., "A Finite Element Model for Composite Beams with Arbitrary Cross-Sectional Warping," *AIAA Journal,* Vol. 26, No. 12, 1988, pp. 1512–1520.

[5]Smith, E. C., and Chopra, I., "Formulation and Evaluation of an Analytical Model for Composite Box Beams," *Proceedings of 31st AIAA/ASME/ASCE/AHS Structures, Structural Dynamics and Materials Conference,* AIAA, Washington, DC, April 1990.

[6]Rehfield, L. W., "Design Analysis Methodology for Composite Rotor Blades," *Proceedings of the Seventh DoD/NASA Conference on Fibrous Composites in Structural Design,* Denver, CO, June 1985.

[7]Rehfield, L. W., Atilgan, A. R., and Hodges, D. H., "Nonclassical Behavior of Thin-Walled Composite Beams with Closed Cross-Sections," *Journal of The American Helicopter Society,* Vol. 35, No. 2, 1990, pp. 42–50.

[8]Nixon, M. W., "Extension-Twist Coupling of Composite Circular Tubes with Application of Tilt Rotor Blade Design," *Proceedings of 28th AIAA/ASME/ASCE/AHS Structures, Structural Dynamics and Materials Conference,* AIAA, Washington, DC, April 1987.

[9]Hodges, D. H., Atilgan, A. R., Fulton, M. V., and Rehfield, L. W., "Dynamic Characteristics of Composite Beam Structures," *AHS National Specialists' Meeting on Rotorcraft Dynamics,* Fort Worth, TX, Nov. 13–14, 1989.

[10]Houbolt, J. C., and Brooks, G. W., "Differential Equations of Motion for Combined Flapwise Bending, Chordwise Bending, and Torsion of Twisted Nonuniform Rotor Blades," NACA Rept. 1346, 1958.

[11]Hodges, D. H., and Dowell, E. H., "Nonlinear Equation of Motion for the Elastic Bending and Torsion of Twisted Nonuniform Rotor Blades," NASA TN D-7818, Dec. 1974.

[12]Srinivasan, A. V., et al., "Structural Dynamics of a Helicopter Rotor Blade System," *Journal of the American Helicopter Society,* Vol. 35, No. 1, 1990, pp. 75–85.

[13]Crawley, E. F., and Luis, J., "Use of Piezo-electric Actuators as Elements of Intelligent Structures," *AIAA Journal,* Vol. 25, No. 10, 1987, pp. 1373–1385.